Geomechanics and Engineering, *Vol. 28, No. 2 (2022) 117-133*
https://doi.org/10.12989/gae.2022.28.2.117

2D numerical study of the mechanical behaviour of non-persistent jointed rock masses under uniaxial and biaxial compression tests

Mojtaba Rabiei Vaziri[1], Hossein Tavakoli[1] and Mojtaba Bahaaddini*[1,2,3]

[1]*Department of Mining Engineering, Shahid Bahonar University of Kerman, Kerman, Iran*
[2]*School of Mining Engineering, College of Engineering, University of Tehran, Tehran, Iran*
[3]*School of Minerals and Energy Resources Engineering, UNSW Sydney, Sydney, Australia*

(Received May 7, 2021, Revised November 12, 2021, Accepted December 1, 2021)

Abstract. Determination of the mechanical behaviour of jointed rock masses has been a challenge for rock engineers for decades. This problem is more pronounced for non-persistent jointed rock masses due to complicated interaction of rock bridges on the overall behaviour. This paper aims to study the effect of a non-persistent joint set configuration on the mechanical behaviour of rock materials under both uniaxial and biaxial compression tests using a discrete element code. The numerical simulation of biaxial compressive strength of rock masses has been challenging in the past due to shortcomings of bonded particle models in reproducing the failure envelope of rock materials. This problem was resolved in this study by employing the flat-joint contact model. The validity of the numerical model was investigated through a comprehensive comparative study against physical uniaxial and biaxial compression experiments. Good agreement was found between numerical and experimental tests in terms of the recorded peak strength and the failure mode in both loading conditions. Studies on the effect of joint orientation on the failure mode showed that four zones of intact, transition to block rotation, block rotation and transition to intact failure occurs when the joint dip angle varies from 0° to 90°. It was found that the applied confining stress can significantly alter the range of these zones. It was observed that the minimum strength occurs at the joint dip angle of around 45 degrees under different confining stresses. It was also found that the joint orientation can alter the post peak behaviour and the lowest brittleness was observed at the block rotation zone.

Keywords: DEM; failure mode; flat-Joint model; mechanical behaviour; non-persistent jointed rock mass

1. Introduction

An essential step prior to design of structures founded in or on rock structures is the estimation of the mechanical behaviour of the hosted rock mass. As the intact material is intersected by sets of discontinuities in the jointed rock mass, the mechanical properties of the rock mass are significantly altered by the presentence of the discontinuities. Estimation of the mechanical properties of the rock mass has been a challenge for rock engineers and engineering geologist for decades. This problem was one of the main reasons for establishment of the International Society for Rock Mechanics (ISRM) in 1962 (Brown 2008). It is widely known that the existing continuum mechanics and soil mechanics methods are inadequate for solving rock mechanics problems in jointed rock masses. This problem is more complex in the case of non-persistent jointed rock mass due to interaction of rock bridges on the failure mechanism and the rock mass strength. Field scale investigations show that most of the discontinuities in the jointed rock masses are non-persistent (Jamil 1992). Performance of the rock mass with non-persistent joints under different loading conditions is significantly controlled by the joint configuration and loading conditions. Most of the existing methods for estimation of the mechanical behaviour of rock masses are based on the persistency assumption while there is a need for fundamental understanding of the failure mechanisms and mechanical behaviour of non-persistent jointed rock masses in many site-scale projects, such as slope stability analyses and the determination of the representative element volume (REV).

Review of previous studies show that the previous researches have been mainly focused on the effect of single or multiple joints on the strength and failure mechanism of rock specimens under different loading conditions (Bobet and Einstein 1998, Park and Bobet 2010, Tian and Yang 2017, Yang *et al.* 2018, Yang and Jing 2011, Yin et al. 2014, Zhang *et al*. 2020). Despite the significant improvement in understanding the stress state, crack initiation, crack propagation and failure mechanism of these materials, joints usually occur in sets in natural rock masses. However, the mechanical behaviour of non-persistent jointed rock mass is more complex, and the mechanical response of each joint is altered by the presence of adjacent joints. A smaller number of studies has been carried out on this topic. These studies can be divided into three main categories of analytical models, physical experiments, and numerical models.

Analytical models for estimation of the mechanical behaviour of non-persistent jointed rock mass are very limited. This limitation is mainly due to difficulties in analytical representation of complex stress state around the

*Corresponding author, Associate Professor
E-mail: m.bahaaddini@ut.ac.ir

ISSN: 2005-307X (Print), 2092-6219 (Online)

crack tips and rock bridges (Elmo *et al*. 2018). The Jennings criterion (1970) is the most widely known analytical model based on limiting equilibrium method where the Mohr–Coulomb criterion was employed to estimate the total shear strength τ in terms of linear combination of the shear strength of rock joints and rock bridges, as follows

$$\tau = k\left(c_j + \sigma_n tan\phi_j\right) + (1-k)(c_r + \sigma_n tan\phi_r) \quad (1)$$

where σ_n is the applied normal stress, $(c_j,\ \phi_j)$ and $(c_r,\ \phi_r)$ are the cohesion and friction angle of joint and intact rock bridges, respectively. The Jennings equation can be expressed in terms of principal stresses $(\sigma_1,\ \sigma_3)$ as follows

$$\sigma_1 = \frac{\left(\frac{2}{sin(2\beta)}\right)\{kc_j+(1-k)c_r\}+\sigma_3[1+\{ktan\phi_j+(1-k)tan\phi_r\}cot\beta]}{1-tan\beta\{ktan\phi_j+(1-k)tan\phi_r\}} \quad (2)$$

where β is the joint angle with respect to the major principal stress. k is the joint persistency factor which is defined in terms of rock bridges and joint lengths $(L_j,\ L_r)$, as follows

$$k = \frac{L_j}{(L_j+L_r)} \quad (3)$$

In the Jennings equation, the effect of joints presence on the stress distribution and progressive failure is ignored and it is assumed that the strength activation of the intact rock bridges and joints occurs simultaneously. Furthermore, it is assumed that the stress is distributed uniformly across intact rock bridges and joints and the interaction of joints is disregarded. To overcome the shortcoming of simultaneous mobilisation of joint and intact rock shear strength, Renani *et al.* (2019) introduced the strength mobilisation factors $(M_j,\ M_r)$ in the Jennings criterion in the following form

$$\tau = M_j k\tau_j + M_r(1-k)\tau_r \quad (4)$$

However, the stress distribution on joints as well as intact rock bridges are not uniform, and no method has been proposed to determine these strength mobilisation factors. Kachanov (1987) based on linear elastic fracture mechanics (LEFM) proposed an analytical solution for stress analysis in elastic solid materials with many cracks.

Results of previous experimental studies have shown that different failure modes may occur in the non-persistent jointed rock mass which is mainly dependent on the joint configuration and the loading conditions. Development of an analytical model without considering the failure mode may result in unrealistic strength estimation of the non-persistent jointed rock mass. Cording and Jamil (1997) developed an analytical model for the step-path failure mode. They noted that the tensile strength of rock bridges σ_t controls the strength of these materials, and they proposed the following strength criterion in terms of shear strength and normal stress as well as principal stresses

$$\tau = \sigma_t \frac{d}{L_j} + \sigma_n\, tan\left(\phi_j + i\right) \quad (5)$$

$$\sigma_1 = \frac{\frac{2\sigma_t d}{sin2(\beta-i)L_j}+\sigma_2\left(1+tan\left(\phi_j+i\right)/cot(\beta-i)\right)}{1-tan\left(\phi_j+i\right)tan(\beta-i)} \quad (6)$$

where i is the equivalent dilation angle $(i = \tan^{-1}(d/L_j))$ and d is the joint spacing. However, comparison of the predicted strength against physical experiments showed a clear overestimation of this analytical approach, especially at low confining stresses (Jamil 1992, Mughieda 1997, Prudencio and Van Sint Jan 2007). Review of analytical efforts clearly show that the developed analytical methods for estimation of the mechanical behaviour of jointed rock masses are very limited due to complex nature of governing equations as well as utilisation of unrealistic assumptions to simplify their mechanical behaviour.

A number of physical experiments have been undertaken on synthetic non-persistent jointed rock materials. Most of these studies have been carried out on synthetic samples containing limited number of fractures to investigate the fracture initiation, propagation and coalescence in terms of wing crack and secondary cracks (Park and Bobet 2009, Wong and Chau 1998). Experimental studies on non-persistent joint sets are limited and most of them have been undertaken under uniaxial compression condition (Asadizadeh *et al*. 2018, Shemirani *et al.* 2017). Jamil (1992) investigated the effect of joint geometry on the failure mode and the strength of a single set of joints through uniaxial and biaxial compression tests. He found four failure modes of planar failure, step-path, multi-plane stepping and intact rock failure in his experiments. Mughieda (1997) carried out uniaxial compression tests on a single plane and multiple planes of a non-persistent joint set and realised that the stresses are distributed more uniformly over the joints and intact rock bridges in the case of multiple planes compared to that of a single plane. Prudencio and Van Sint Jan (2007) carried out a comprehensive uniaxial and biaxial compression tests on synthetic samples prepared from a mixture of cement, sand and water which was intersected by a single set of non-persistent joints having different joint configurations and proposed an empirical equation for estimation of the strength. They noted the empirical constants of the proposed equation should be determined based on the joint configuration parameters where no suggestion was made at different scenarios. Furthermore, the influence of failure mode on the empirical model was ignored. Chen *et al*. (2012) investigated the influence of joint orientation and joint persistency factor on deformation behaviour of jointed rock masses through uniaxial compression tests on synthetic specimens containing a single set of non-persistent open joints. They found that the failure mechanism is significantly controlled by the joint orientation rather than the joint persistency factor. Yang *et al*. (2017) through uniaxial compression tests on synthetic jointed materials, which were made up of plaster, investigated the effect spacing and joint overlap of parallel joints at different dip angles on the strength and failure mechanism. Han *et al*. (2018) investigated the effect of joint orientation on the strength, failure mode and deformation modulus of resin infilled parallel fractures in cemented materials under uniaxial and biaxial compressions. They observed W-shaped variation of strength with an increase in the joint set dip angle in uniaxial compression tests while for biaxial tests, V-shaped strength variation was observed. Review of experimental studies show that most of these experiments were performed on rock-like materials where special difficulties exist in preparation of the samples and a limited

number of synthetic samples can be prepared in each set of experiments. However, several geometrical parameters control the behaviour of these materials and repetition of the experiments is the other challenging task.

Recent developments in computer technology and the consequent significant improvements in numerical simulation of materials provide an opportunity to understand the complicated mechanical behaviour of the non-persistent jointed rock masses. Due to discontinuous nature of these materials and deficiencies of constitutive models for estimation of stress state around non-persistent joints, most of the previous numerical studies have been undertaken using the discrete element method (DEM) (Tian and Yang 2017, Zhao *et al*. 2015). Vergara *et al.* (2016) employed the Voronoi model in the UDEC code to study the failure mechanism and strength of non-persistent jointed rock masses. In the Voronoi model, the intact material is simulated by polygonal blocks bonded at their boundaries and fracturing is restricted at the blocks' boundaries (Bahaaddini and Rahimi 2018). Therefore, the failure mechanism is dependent on the size of polygonal blocks which is a restricting issue at the current stage. Particle flow code (PFC) is the most widely used numerical approach for simulation of jointed rock masses where the intact material is simulated by assemblies of circular (2D) or spherical (3D) particles bonded at their contact points. Fan *et al.* (2015) studied the influence of multi-non-persistent joints configuration on uniaxial compressive strength (UCS) and deformation modulus. They found that the occurrence of minimum strength and deformation modulus at different joint orientations is dependent on the joint persistency factor while the joint stiffness has no significant effect on the mechanical behaviour of these materials. Cao and Lin (2017) studied the influence of multiple sets of joints having different joint configuration on the uniaxial strength, failure pattern, and the strain energy. Bahaaddini *et al.* (Bahaaddini 2014, Bahaaddini *et al*. 2011, Bahaaddini et al. 2012b) in a comprehensive study investigated the effect of joint configuration on the strength, deformation modulus and failure mode through parametric studies and statistical analyses. Bahaaddini *et al*. (2013) investigated the ability of the parallel bond (PB) model in reproducing the strength of intact rock and non-persistent jointed samples under different biaxial loading conditions through a comparative study against physical experiments. They found that the PB model underestimates the strength of non-persistent jointed rock material and this discrepancy increases with an increase in the confining stress. Therefore, they limited their analyses to only uniaxial compression tests due to shortcomings of the PB in reproducing of the intact rock failure envelope.

In the previous numerical studies using PFC, the intact material has been simulated using the PB model. It is widely known that the PB model is not able to reproduce the tensile strength and slope of failure envelope of intact rock materials. This problem is mainly related to circular shape of particles and excessive rotational forces at contact points (Potyondy 2011, 2012, Potyondy and Cundall 2004). Therefore, the numerical simulations of the mechanical behaviour of non-persistent jointed rock masses under confining stresses in PFC have been challenging in the previous studies.

This paper aims to numerically study the effect of joint configuration on the mechanical behaviour of non-persistent jointed rock masses under both uniaxial and biaxial compression tests using a DEM code, PFC2D. To overcome the shortcomings of conventional bonding approaches in PFC, the flat-joint (FJ) bonding model was employed. Firstly, a validation study was undertaken through a comparative study against physical uniaxial and biaxial compression experiments undertaken by Prudencio and Van Sint Jan (2007). The mechanical properties of the bonded particle model were calibrated using direct tensile, uniaxial and biaxial compression tests and the joint micro-parameters were calibrated using the normal deformability and the direct shear tests. Then, numerical models similar to physical samples (Prudencio and Van Sint Jan 2007) were prepared and uniaxial and biaxial compression tests were undertaken. Finally, the effect of joint orientation on the strength, deformation modulus and post-peak behaviour under different loading conditions was investigated.

2. Numerical simulation of the intact rock and discontinuities in PFC

In the PFC, the intact rock is simulated using circular (in 2D) or spherical (in 3D) particles bonded together. The generated numerical specimen is called bonded particle model (BPM). The bond between particles plays a significant role in the mechanical behaviour of rock materials. Three main bonding approaches have been developed for simulation of the BPM, namely contact bond (CB), parallel bond (PB) and flat-joint (FJ) models (Itasca Consulting Group. Inc 2015). The main differences between the CB and the PB models are illustrated in Fig. 1. The CB is only active at the contact point and it can only transmit the applied force between particles while the PB is active over a finite cross-section (rectangle in 2D or disc in 3D) at the contact plane and both force and moment can be transmitted between particles. Therefore, the PB can resist bending moment and oppose rolling (Cho *et al.* 2007). Despite the ability of the PB in reproducing many features of rock materials in laboratory and field scale, underestimation of the failure envelope slope as well as overestimation of the tensile strength are the main restricting issues in the PB modelling of rock materials. This problem is mainly due to circular shape of particles in the PB models where the grain interlocking cannot be simulated due to lack of moment resistance and excessive rotation of particles after the bond breakage (Bahaaddini *et al.* 2019, Potyondy 2015). However, by introduction of the newly developed flat-joint (FJ) model, the above noted restrictions have been resolved.

2.1 Flat-joint model

The FJ model was proposed by Potyondy (2012) to eliminate the intrinsic shortcomings of circular shape of particles by considering polygonal grain structure. The FJ contact is visualised by local flat notional surfaces placed at the contact point and joined to the particles, as schematically shown in Fig. 2. The particle notional surface interacts with the notional surface of the contacting piece. Thus, each faced particle is depicted as a core with

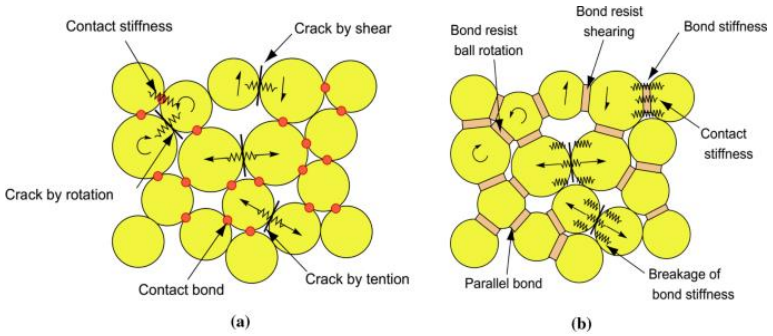

Fig. 1 Comparison between the contact bond (CB) and the parallel bond (PB) models (a) CB model and (b) PB model (Cho *et al.* 2007)

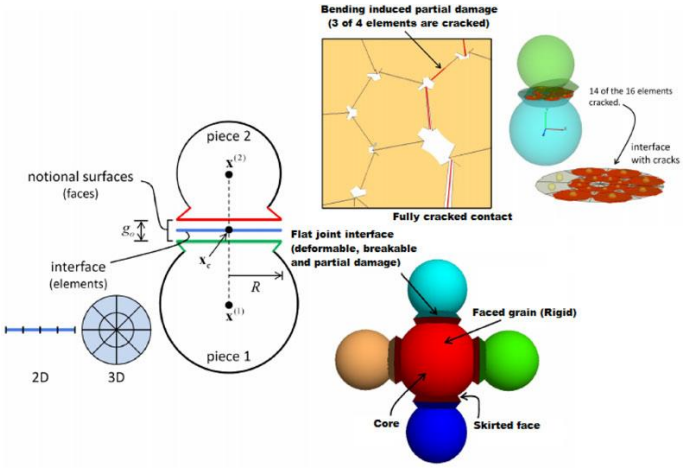

Fig. 2 Simulation of the intact material using the flat-joint model (Potyondy 2015)

skirted faces. The interface between faced particles (line in 2D or disk in 3D) is discretised into elements and each element can be either bonded or unbonded. This characteristic enables the simulation of pre-existing cracks in the flat-jointed material (Itasca Consulting Group. Inc 2015).

After the FJ bond installation, the force and moment values for each element are set to zero and updated according to the force–displacement law. The normal force is updated directly based on the linear elastic model while the shear force is updated in an incremental mode. The maximum normal and shear stresses ($\sigma_M^{(e)}$ and $\tau_M^{(e)}$) at each element are calculated as follows

$$\sigma_M^{(e)} = \frac{-\bar{F}_{(e)}^n}{A^{(e)}} \tag{7}$$

$$\tau_M^{(e)} = \frac{\bar{F}_{(e)}^s}{A^{(e)}} \tag{8}$$

where $A^{(e)}$ is the element area and $\bar{F}_{(e)}^n$ and $\bar{F}_{(e)}^s$ are the applied normal and shear forces on the element, respectively. The strength of the bonded element follows the Coulomb model having tensile cut-off. When the maximum tensile stress exceeds the element tensile strength, element breaks in tension and the status of the element changes to unbonded. The shear strength of element is controlled by the FJ cohesion c_b and friction angle $\emptyset_b$. When the maximum shear strength exceeds the element shear strength ($\tau_b = c_b + \bar{\sigma}\tan\emptyset_b$), element breaks in shear and the status of the element changes to unbonded with residual strength (Itasca Consulting Group. Inc 2015).

The mechanical behaviour of unbonded element is defined by linear elastic model with frictional slip, as follows

$$\bar{\sigma} = \begin{cases} 0 & \overline{g} \geq 0 \\ -\bar{k}_n \overline{g} & \overline{g} < 0 \end{cases} \tag{9}$$

$$\bar{\tau} = \begin{cases} -\overline{\sigma}\ tan\varphi_r & \overline{\sigma} < 0 \\ 0 & \overline{\sigma} = 0 \end{cases} \tag{10}$$

where $\overline{g}$ is the element gap, φ_r is the residual friction angle and $\bar{k}_n$ is the bond normal stiffness. The breakage of each element leads to partial damage of the FJ contact. Therefore, the FJ contact bonding status can be partially damaged, fully bonded and unbonded with frictional status, as shown in Fig. 2. This characteristic enables the resistance against relative rotation of particles even for fully broken interface which was problematic in the CB and PB models. Furthermore, the initial bonded and unbonded status of elements offers the simulation of pre-existing cracks in the material (Bahaaddini *et al.* 2019, Potyondy 2015, Wu and Xu 2016).

As the relative displacement at a FJ contact exceeds the FJ diameter, the notional faces are deleted. If these particles

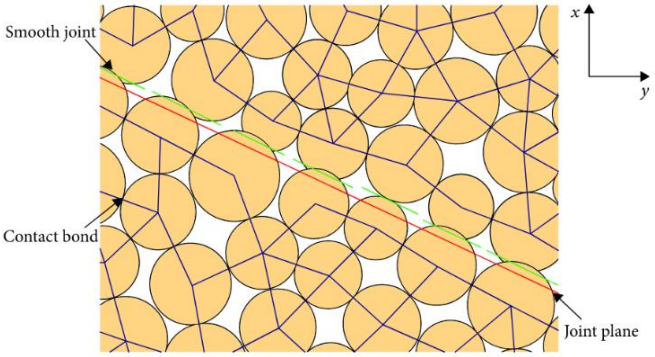

Fig. 3 Simulation of joint interfaces using the smooth joint contact model (Bahaaddini 2014)

come back into contact, their mechanical behaviour is that of the linear contact model (Potyondy 2012). Recent studies have shown that the FJ model can reproduce the mechanical behaviour of rock materials under different loading conditions and the intrinsic problems of CB and PB models in reproducing the tensile strength and triaxial compressive strength of rock materials has been resolved in this model (Bahaaddini *et al.* 2019, Wu and Xu 2016).

2.2 Smooth joint model

Originally, joints have been simulated in the PFC by removing bonds between particles which lie on the joint interface and assigning a low friction coefficient to these unbonded particles (Cundall 2000, Mas Ivars *et al*. 2011). However, the bond removal method results in inherent bumpiness of the joint surface at the grain scale and the consequent unrealistic shear behaviour and dilation (Bahaaddini *et al*. 2012a). The smooth joint (SJ) model was introduced by Cundall (Pierce *et al*. 2007) to resolve these issues where after removing bond between particles lying on the joint plane, small scale SJ contacts are assigned between these particles, as shown in Fig. 3. The SJ contact is assigned between particles which their centres lying on the opposite sides of the joint plane. Particles having SJ contact may overlap or pass through each other rather than being restricted to move around one another (Pierce *et al*. 2007). The SJ is active as long as the particles remain in contact (Itasca Consulting Group. Inc 2015).

The properties of the SJ are defined by the coefficient of friction μ_j, dilation angle ψ_j, normal stiffness $\bar{k}_{nj}$ and shear stiffness $\bar{k}_{sj}$. The force-displacement at SJ contacts obey linear elastic model having the Coulomb shear strength model with dilation. Normal and shear forces (F_n, F_s) are updated at the end of each calculation cycle (Itasca Consulting Group. Inc 2015).

If the updated shear force $|F_s'| \leq F_s^* = F_n\mu_j$, then $|F_s| = |F_s'|$ and the normal and shear forces are updated as follows

$$F_n := F_n + \bar{k}_{nj} A \Delta U_n^e \tag{11}$$

$$F_s' := F_s - \bar{k}_{sj} A \Delta U_s^e \tag{12}$$

where F and U are relative force and displacement and subscripts n and s denote normal and shear components in the local coordinate system of the joint plane, respectively. If the updated shear force exceeds the sliding shear strength $|F_s'| > F_s^*$, then sliding occurs and normal and shear forces are updated as follows (Itasca Consulting Group. Inc 2015)

$$|F_s| = F_s^* \tag{13}$$

$$F_n := F_n + A\Delta U_s^* \bar{k}_{nj} \tan\psi_j = F_n + \left(\frac{|F_s'| - F_s^*}{\bar{k}_{sj}}\right) \bar{k}_{nj} \tan\psi_j \tag{14}$$

In the SJ model, a contact gap can be defined and by closure of the gap under the applied normal stress, the SJ status changes to active. This characteristic enables the simulation of initial aperture in rock joints.

3. Validation study

The validity of numerical approach was investigated through a direct comparison against physical experiments undertaken by Prudencio and Van Sint Jan (2007). Numerical specimens having different joint configurations were prepared. The geometrical parameters of these samples under biaxial compression tests are schematically shown in Fig. 4. Ten series of prismatic specimens having 150 width and 300 height were prepared. The joint geometrical parameters of these samples are summarised in Table 1 and Fig. 5. It should be noted that experiments of series A were undertaken on intact prismatic samples where the experimental properties were used for the calibration of FJ micro-parameters as explained in the following section. Prudencio and Van Sint Jan (2007) prepared non-persistent jointed rock masses by inserting 0.1 mm thick steel sheets into the mortar mixture and they were removed after 24 hours. Samples were cured 14 days in a room with controlled humidity and temperature.

As the micro-properties of the bonded particle models cannot be measured directly in the laboratory-scale, an essential step prior to the numerical analysis is the calibration of micro-parameters (Zhou *et al.* 2018). The micro-properties of the FJ model were calibrated by simulation of direct tension, uniaxial and triaxial

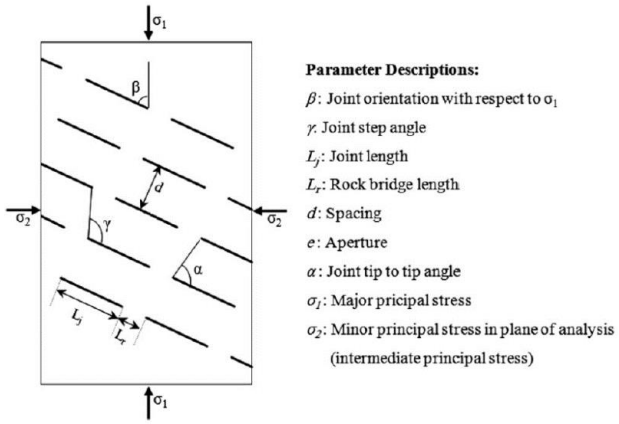

Fig. 4 Joint geometrical parameters of the numerical specimens (Prudencio and Van Sint Jan 2007)

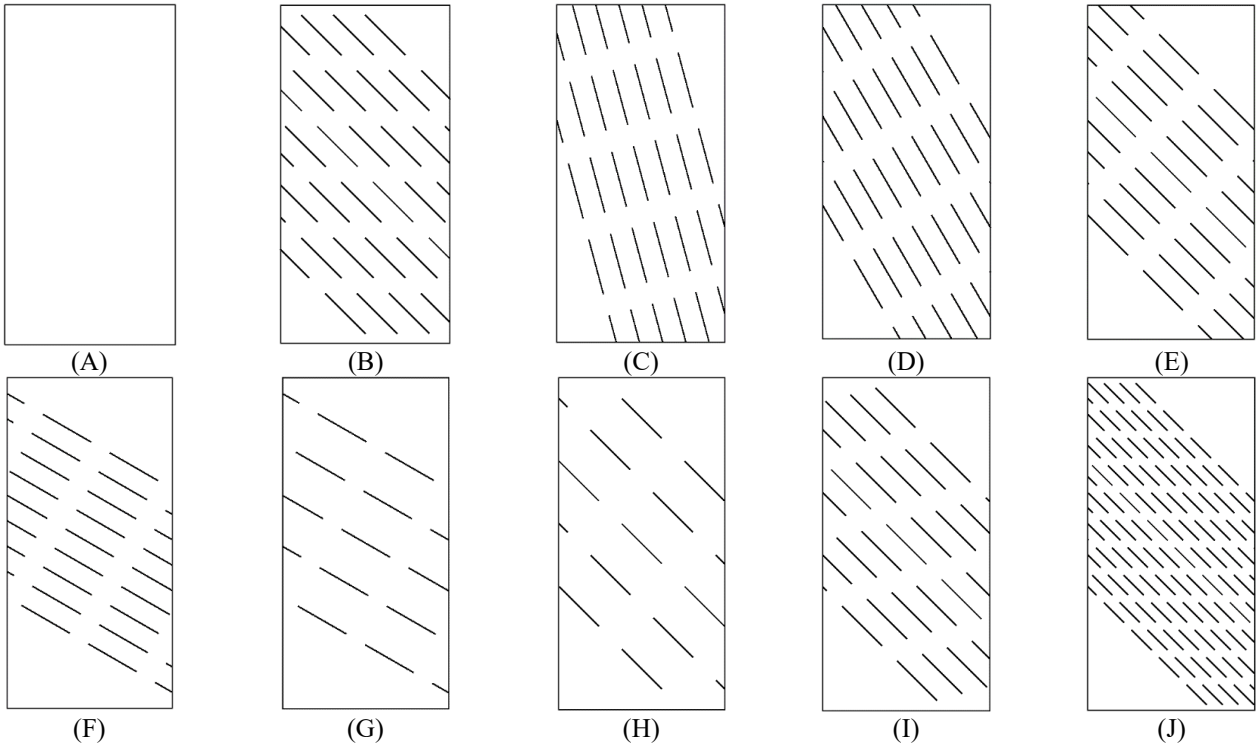

Fig. 5 Schematic view of generated non-persistent jointed samples (Prudencio and Van Sint Jan 2007)

Table 1 Joint geometrical parameters of the numerical specimens (Prudencio and Van Sint Jan 2007)

Series	L_j (mm)	L_r (mm)	d (mm)	γ (°)	β (°)	e (mm)
A	---	---	---	---	---	---
B	50	20	20	90	45	0.1
C	50	20	20	135	15	0.1
D	50	20	20	135	30	0.1
E	50	20	20	135	45	0.1
F	50	20	20	135	60	0.1
G	50	20	40	117	60	0.1
H	50	30	40	127	45	0.1
I	50	20	20	113	45	0.1
J	25	10	10	90	45	0.1

compression tests and the SJ micro-parameters were calibrated by direct shear tests and normal deformability tests. After the calibration of micro-parameters, ten series of non-persistent jointed samples were prepared, and uniaxial and biaxial compression tests were undertaken.

3.1 Calibration of the intact material

Numerical samples having the width of 150 mm and height of 300 mm, similar to physical experiments, were prepared in PFC2D. In the sample generation process, first a vessel consists of frictionless walls is created and this vessel is filled up by randomly placed particles. The minimum radius (R_{min} = 0.5 mm) and the ratio of maximum to minimum radius (R_{max}/R_{min} = 1.5) are assigned and particles having normal distribution sizes are generated. After generation of the particle assembly, a specified isotropic stress is applied between particles, in a grain scaling process, to create well-connected particles and reduce the amount of locked in stresses. In the final step, FJ bonds are installed at the grain–grain contacts having a contact gap less than or equal to the installation gap (Itasca Consulting Group. Inc 2015).

The calibration process of the FJ micro-parameters was carried using direct tensile, uniaxial and biaxial compression tests to reproduce the mechanical properties of the intact material measured in the laboratory. The numerical set-up for these experiments is shown in Fig. 6. In the uniaxial compression test, the side walls were deleted, and the upper and lower walls were used to simulate the axial loading frame where they moved under a constant displacement rate of 0.0075 m/s towards each other's. In the biaxial compression tests, a specified confining stress was applied using the side walls and their velocity was controlled by a servo-control mechanism to maintain the pre-designed confining stress in the loading process. To perform the direct tensile test, specified regions in the top and bottom parts of the sample were gripped and the sample was pulled from both sides.

The calibration process was undertaken in an iterative process followed by the methodology suggested by Bahaaddini *et al.* (2019). Firstly, an appropriate number of elements were chosen for FJ contacts (2 to 4 elements was suggested (Bahaaddini *et al.* 2019)). In the initial stage of calibration, the FJ cohesion was set to a high value to forbid the initiation of pre-mature cracks. Then, the FJ-bonded fraction and the FJ tensile strength were calibrated through direct tensile test. Then, the particle and the FJ bond normal to shear stiffness ratios (k_n/k_s and $\bar{k}_n/\bar{k}_s$) were calibrated in the uniaxial compression test to reproduce the laboratory measured Poisson's ratio. In an iterative process with the previous stage, the Elastic modulus was reproduced by changing the particle and the bond Elastic modulus ($E_c$and $\bar{E}_c$). Then, the uniaxial compressive strength (UCS) was reproduced by varying the FJ cohesion. Finally, the biaxial compression tests were undertaken at different confining stresses and the experimental intact friction angle was recovered by changing the FJ friction angle and the friction coefficient of unbonded contacts. The calibrated micro-parameters of particles and FJ bonds are summarised in Tables 2. Results of numerical direct tensile, uniaxial and biaxial compression tests are compared with experimental tests in Table 3. These results show a good agreement between the FJ bonded model and experimental results. The results of biaxial compression tests for the calibrated numerical model under different confining stresses are illustrated in Fig. 7. These results clearly show that the increase in the lateral confining stress results in the change of the post-peak behaviour from brittle to ductile failure mode.

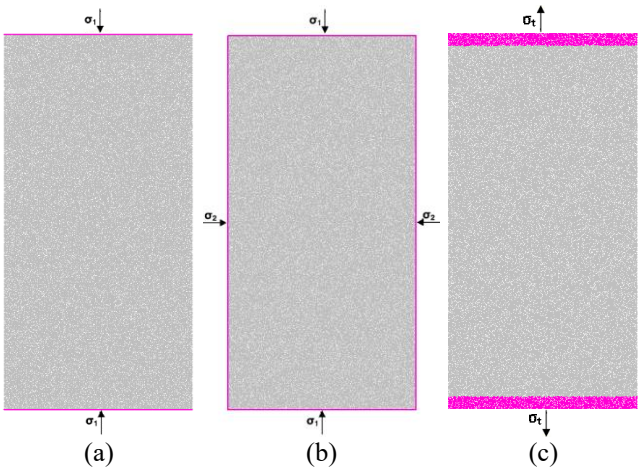

Fig. 6 Numerical simulation of experiments to calibrate the FJ micro-properties (a) Uniaxial compression test and (b) Biaxial compression test and (c) Direct tension test

Table 2 Calibrated micro-parameters of the particles and the FJ contact

Micro-properties of Particles		Micro-properties of the Flat-joint contacts	
density (kg/m^3)	2100	Installation gap (mm)	0.2
E_c (GPa)	2.08	$\bar{E}_c$ (GPa)	2.08
k_n/k_s	1.8	$\bar{k}_n/\bar{k}_s$	1.8
R_{min} (mm)	0.5	Bonded fraction	0.83
R_{Max}/R_{min}	1.5	Number of elements	4
Friction coefficient, μ	0.49	Tensile strength (MPa)	1.48
		Cohesion (MPa)	1.82
		Friction angle (º)	20

Table 3 Comparison of the result of calibrated FJ models against physical experiments (series A)

	UCS (MPa)	*E* (GPa)	υ	σ_t (MPa)	*c* (MPa)	φ (º)
Numerical	3.87	2.404	0.166	0.52	0.95	37
Experimental	3.84	2.4	0.16	0.45	0.86	40.9

3.2 Calibration of the smooth joint parameters

As noted earlier, the SJ parameters include SJ normal stiffness ($\bar{k}_{nj}$), SJ shear stiffness ($\bar{k}_{sj}$), SJ friction coefficient (μ_j) and SJ dilation angle (ψ_j). Bahaaddini *et al.* (2015) in a parametric study on the effect of SJ parameters

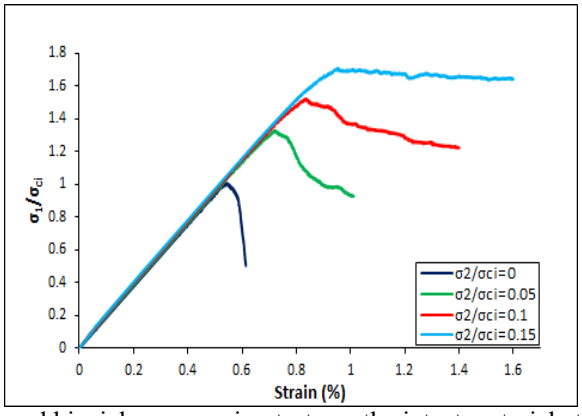

Fig. 7 Results of numerical uniaxial and biaxial compression tests on the intact material at different confining stresses and the change of post-peak behaviour from brittle to fully ductile with the increase in the confining stress

(a) (b)

Fig. 8 Numerical experiments to calibration smooth joint parameters (a) Normal deformability test and (b) Direct shear test

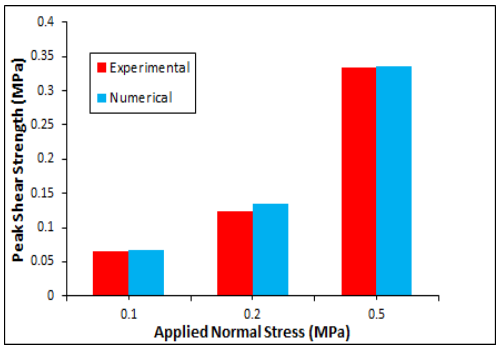

Fig. 9 Comparison of the numerical and experimental peak shear strengths in the direct shear tests under different normal stresses

on the shear behaviour of real and saw-tooth joints showed that the ψ_j should to be chosen 0 to produce valid dilative behaviour. Therefore, in this study the ψ_j was set to zero. The $\bar{k}_{sj}$ and the μ_j were calibrated by undertaking direct shear tests under different constant normal stress and the $\bar{k}_{nj}$ was calibrated by undertaking normal deformability tests to reproduce the experimental behaviour of planar joints (Prudencio 2009, Prudencio and Van Sint Jan 2007).

In these numerical experiments, specimens having the length of 50 mm and height of 40 mm were produced and a planar joint was inserted at mid height of the sample. In the normal deformability test, as shown in Fig. 8(a), lateral walls were removed, and the applied normal stress and the corresponding normal displacement were recorded in the loading process. The $\bar{k}_{nj}$ was determined in trial-and-error process to reproduce the measured joint normal stiffness at the laboratory scale. In the direct shear tests, as shown in Fig. 8(b), the upper block was moved horizontally with a displacement rate of 0.005 m/s and the lower block was kept stationary. A constant normal stress was applied to the upper block and the normal stress was keep constant during the shearing process by using a servo control mechanism (Itasca Consulting Group. Inc 2015). The $\bar{k}_{sj}$ controls the slope of the shear stress-shear displacement graph while the μ_j controls the initiation of sliding in this graph. These parameters were varied to reproduce the peak shear strength and shear stiffness recorded in the laboratory. The measured peak shear strengths at different normal stresses are compared against the physical experiments in Fig. 9. The calibrated SJ parameters are summarised in Table 4. Results of numerical normal deformability and direct shear tests are compared with experimental tests in Table 5, which show a good agreement.

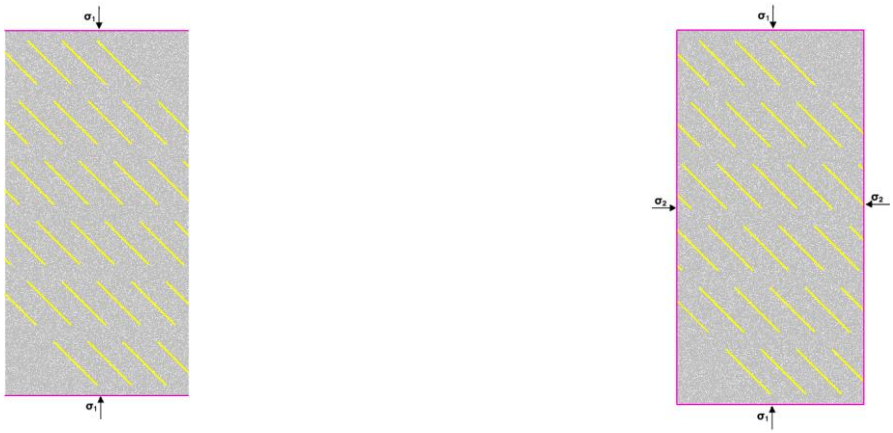

(a) (b)

Fig. 10 A typical non-persistent jointed rock mass model (a) Uniaxial compression test and (b) Biaxial compression test

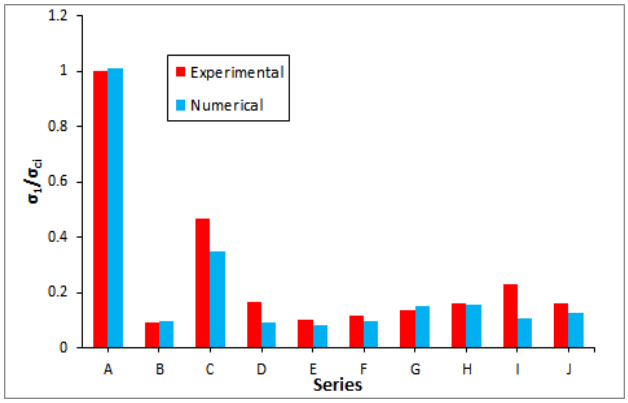

Fig. 11 Comparison the normalised uniaxial compressive strength of numerical and experimental tests for different series

Table 4 Calibrated micro-parameters of the smooth joint model

Smooth joint properties	Calibrated value
$\bar{k}_{nj}$ (GPa/m)	23
$\bar{k}_{sj}$ (GPa/m)	1.39
μ_j	0.67
ψ_j (°)	0

Table 5 Comparison of the result of calibrated numerical normal deformability and direct shear tests with physical experiments

	K_n (GPa/m)	K_s (GPa/m)	φ_j (°)
Numerical	23	1.67	33.8
Experimental	22	1.6	33

3.3 Numerical experiments on non-persistent jointed rock masses

After calibration of the FJ and SJ micro-parameters, numerical specimens similar to physical specimens of Prudencio and Van Sint Jan (Prudencio 2009, Prudencio and Van Sint Jan 2007) were generated and uniaxial and biaxial compression tests were undertaken on these samples. Each sample consists of around 32,500 particles. Joints were generated by defining the coordinates of joint tips for each non-persistent jointed specimen and the smooth contact model was assigned for particles which positioned in either side of the joint surface. A typical generated non-persistent jointed sample (Type B) is shown in Fig. 10.

3.3.1 Uniaxial compression tests

Uniaxial compression tests were carried out on nine sets of non-persistent jointed rock mass and results were compared with the experimental tests, as shown in Fig. 11. To examine the strength reduction in non-persistent jointed rock samples compared to intact material, the measured UCS values were normalised by the UCS of intact specimens (σ_{ci}). This comparison shows that there is a good agreement between the UCS of numerical models and experimental tests.

The failure modes of numerical experiments are illustrated in Fig. 12. Four typical failure modes of step-path, planar, block rotation and the mixed of block rotation and step-path failure were observed in these experiments. The failure modes of numerical models are compared against physical experiments of Prudencio and Van Sint Jan (Prudencio 2009, Prudencio and Van Sint Jan 2007) in Table 6 which shows a good agreement between the results. Numerical failed samples are compared with the reported experimental failure modes of series B, C, E and G in Fig.

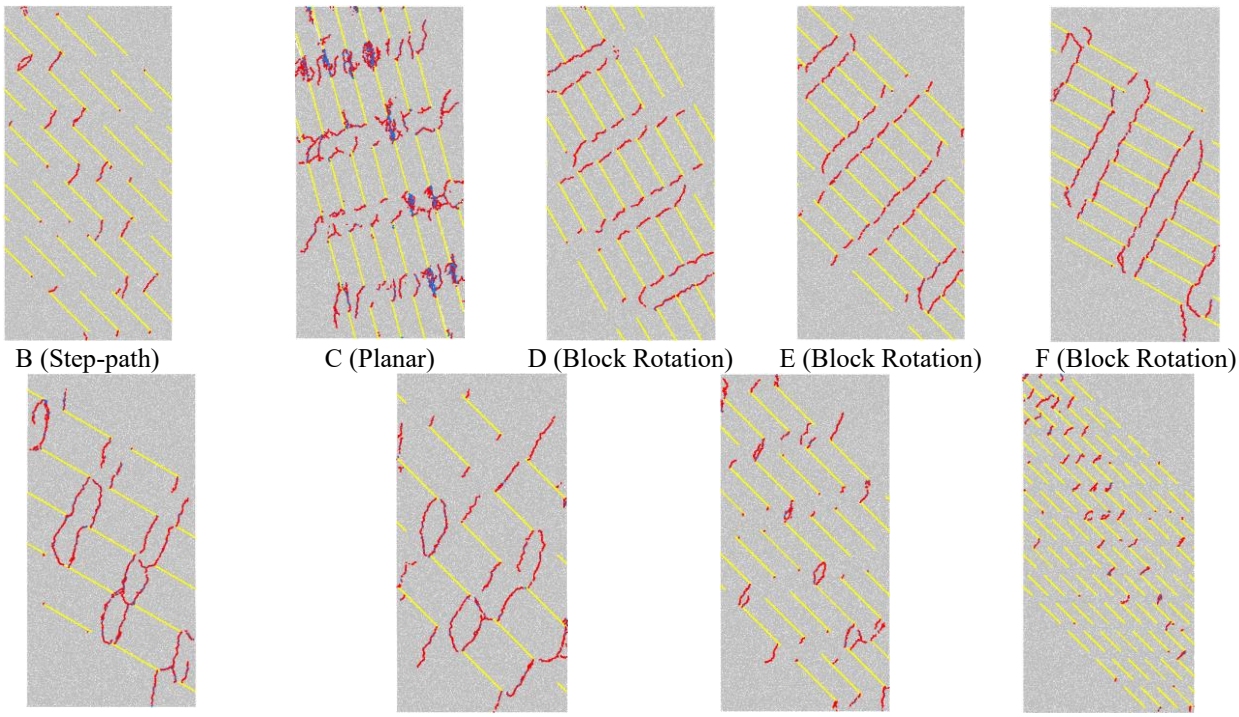

Fig. 12 Failure mechanisms of the numerical experiments under uniaxial compression loading (Yellow line: smooth joint contacts, red: tension crack and blue: shear crack)

Table 6 Comparison between the failure mode of experimental and numerical tests under uniaxial compression tests

Serie	Experimental	Numerical
B	S	S
C	P	P
D	B	B
E	B	B
F	B	B
G	B, B + S	B + S
H	B, B + S	B + S
I	S	S
J	S	S

S= Step-path, P= Planar, B= Block Rotation

13. Comparison between the numerical and experimentally failure modes clearly shows the ability of numerical approach in reproducing the failure mode of non-persistent jointed samples.

The joint orientation β was varied from 15° to 60° in series C, D, E and F while other geometrical parameters were kept constant. The highest uniaxial compressive strength in this range was recorded at β = 15°, and the minimum strength was measured at β = 45° in both experimental and numerical models. The increase of β from 15° to 60° resulted in the change of failure mode from planar to block rotation. In the planar failure mode, tensile cracks initiate from the tips of pre-existing joints and propagate through the rock bridges to reach the adjacent co-linear joints. Wing cracks have the tendency to initiate and propagate perpendicular to the joint planes while the position of adjacent joints and distribution of stresses around the joint tip due to the joint orientation leads to the coalescence of initiated fractures. This failure mode starts with generation of tensile cracks while after propagation of these cracks, shear cracks are generated, as can be observed for the specimen type C (Fig. 12). In the block rotation failure mode, wing cracks initiate from the pre-existing joint tips and propagate perpendicular to the joint orientation. As the stresses are concentrated at the joint tips, the propagation of tensile wing cracks is directed to the next raw of joints where the new rock blocks are generated. As the initiation and propagation of tensile cracks control the failure mechanism, the mechanical behaviour and the strength dependency to the joint orientation is significantly different from that of persistent joints where the minimum strength occurs at joint orientation close to the joint friction angle. In series B, I and J samples failed in the step-path mode. In the step-path failure mode, after the generation of wing cracks and propagating perpendicular to the joint planes, they reach to the tip of the parallel joint system and step-paths failure surfaces are generated. Therefore, this failure mode is the result of tensile fracturing of rock bridges and sliding along the pre-existing joints. In series G and H mixed failure mode occurred (block rotation and step-path failure). In this failure mode, the orientation of co-planar joints as well as joint spacing leads the initiated and propagated wing cracks deviate in the final stages of failure due to redistribution of stresses in the sample which lead to occurrence of the mixed failure mode.

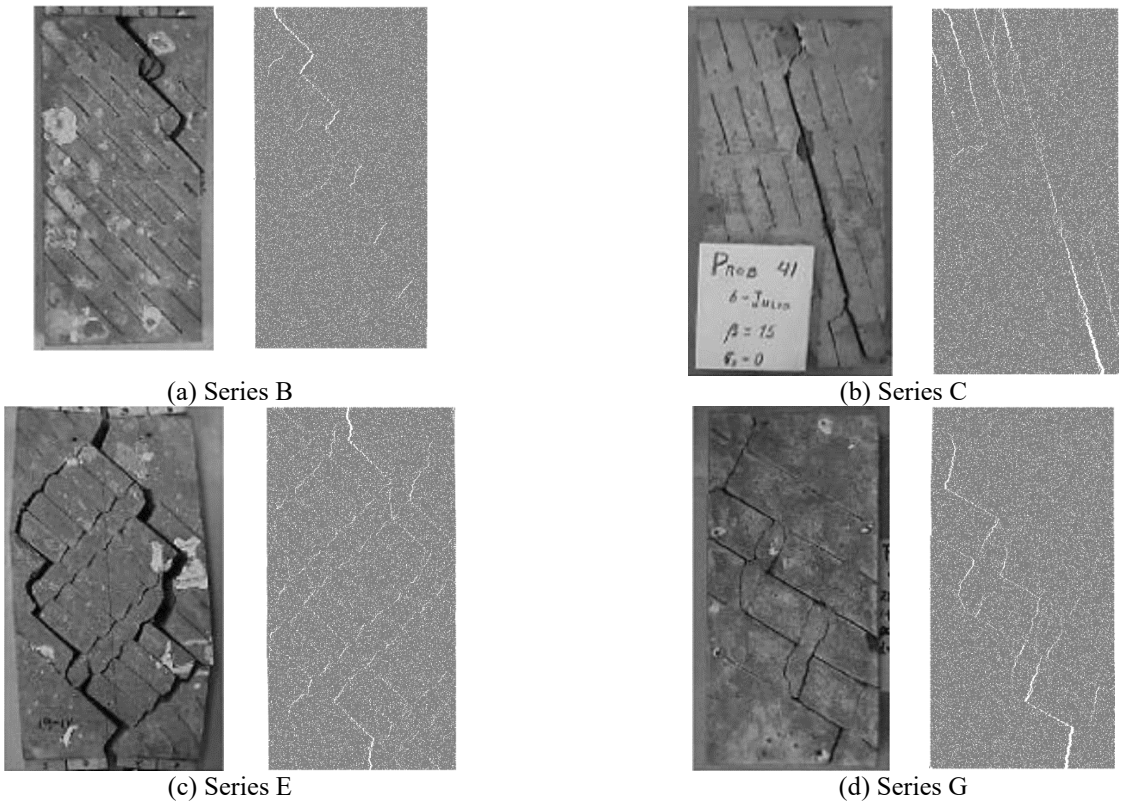

(a) Series B (b) Series C

(c) Series E (d) Series G

Fig. 13 Comparison between the failure mode of experimental (Prudencio 2009) and numerical tests under uniaxial compression test: (a) Type B (Step-path Failure), (b) Type C (Planar Failure), (c) Type E (Block Rotation Failure) and (d) Type G (Block Rotation and Step-path Failure)

3.3.2 Biaxial compression tests

As explained earlier, numerical simulation of the biaxial compression tests of rock materials has been challenging in PFC due to deficiencies of bonding approaches in reproducing the slope of failure envelope. In this study, the ability of the FJ model in reproducing the biaxial compressive strengths of non-persistent jointed samples under different confining stresses were investigated through a comparative study against physical experiments undertaken by Prudencio and Van Sint Jan (Prudencio 2009, Prudencio and Van Sint Jan 2007). Numerical biaxial compression tests were carried out on seven series of samples which their experimental data were available. Numerical experiments were undertaken under different confining stresses in the σ_2/σ_{ci} range of 0 to 0.2 and the results are compared against physical experiments in Fig. 14. There is good agreement between numerical and experimental results at low, medium and high σ_2/σ_{ci} stresses. The failure modes of numerical models at four different σ_2/σ_{ci} are depicted in Fig. 15.

It is observed that an increase in the confining stress results in an increase in the ratio of shear to tensile cracks. It was observed that in series B, the failure mode at low intermediate principal stresses is step-path failure while the increase in the confining stress results in the change of failure mode to mixed step-path and planar failure. In series C, at low confining stresses samples fail in planar failure mode and the increase in the confining stress leads to an increase in the contribution of intact material and generation of more cracks in intact material and consequently intact rock failure at high confining stresses. In series D, E and F ($\beta = 30^{\circ} - 60^{\circ}$) the failure mode is block rotation at low normal stresses while the increase in the confining stress results in the more contribution of intact rock bridges in the failure mode. Therefore, the failure modes in series D ($\beta = 30^{\circ}$) changes to mixed block rotation and planar failure and then to mixed block rotation and intact failure. In series E ($\beta = 45^{\circ}$), the failure mode remains block rotation failure at the investigated range of confining stresses. In series F ($\beta = 60^{\circ}$), the failure mode changes to mixed block rotation and intact failure, and at high confining stresses, the failure mode is mainly controlled by the intact rock bridges failure. In series H, the increase in the confining stress results in the change of failure mode from mixed block rotation and step-path to mixed block rotation and intact failure, and at high confining stress to intact failure. In series I, the failure mode remains step-path failure in the investigated range of confining stresses.

4. Effect of joint orientation on the mechanical behaviour of non-persistent jointed rock masses

As noted earlier, numerical modelling provides an opportunity to understand the complicated mechanical behaviour of non-persistent jointed rock masses while this is challenging in experimental tests due to special difficulties in sample preparation and limitations in the

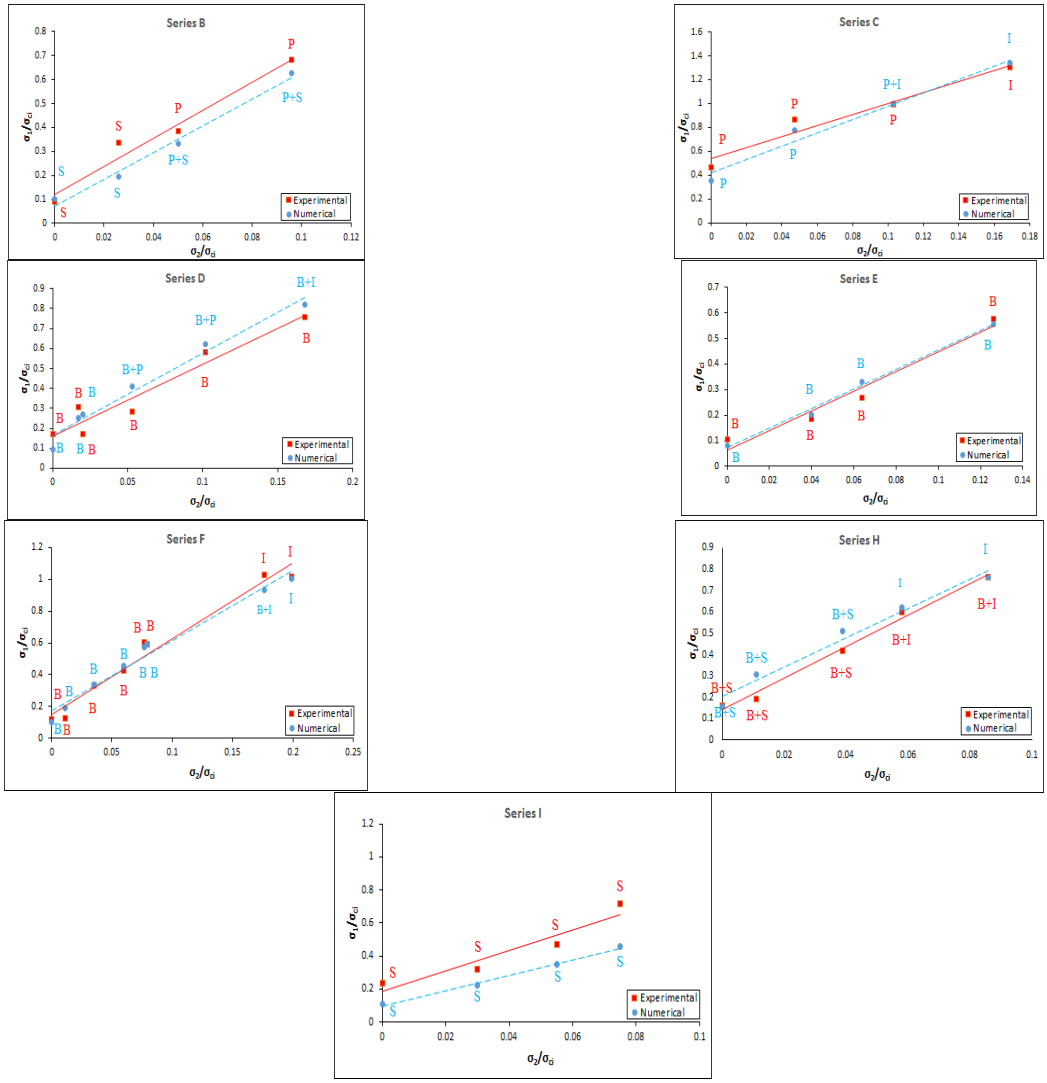

Fig. 14 Comparison of the experimental and numerical biaxial compressive strengths in different series

number of experiments and their repetition. Results of previous section clearly shows that the FJ model is able to reproduce the mechanical behaviour of non-persistent jointed rock masses under different loading conditions. The joint orientation angle is one of the most effective parameters on the mechanical behaviour of non-persistent jointed rock mass (Bahaaddini *et al.* 2013, Bahaaddini *et al.* 2012b). However, most of previous studies has been limited to few joint orientation angles under uniaxial compression tests and the effect of confining stresses on the mechanical behaviour of these materials has not been well studied.

Numerical specimens having the joint orientation angles of 0, 15, 30, 45, 60, 75 and 90 degrees were generated and the mechanical behaviour of these materials under uniaxial and biaxial compression tests at the confining stress ratios of σ_2/σ_{ci} = 0, 0.05, 0.1 and 0.15 were investigated. The stress-strain curves for different joint orientation angle at confining stress ratios of σ_2/σ_{ci} = 0 and 0.1 are depicted in Fig. 16. Investigation of the post-peak behaviour of these samples under uniaxial compression tests (Fig. 16(a)) shows that at $\beta = 0^{\circ}$and 15°(intact and planar failure modes) samples failed in the brittle mode while the change of failure mode at $\beta = 30^{\circ}-75^{\circ}$ (block rotation) resulted in a decrease in the brittleness. At $\beta = 90^{\circ}$ due to breakage of intact rock bridges between the joint planes, the brittleness increases compared to those of block rotation failure modes. Increase in the confining pressure to σ_2/σ_{ci} = 0.1 (Fig. 16(b)) resulted in a decrease in brittleness in all joint orientation angles. Interestingly, the failure mode at $\beta = 30^{\circ}-75^{\circ}$ changed to fully ductile. As the vertical joints ($\beta = 0^{\circ}$) have the lowest effect on the mechanical behaviour of jointed material, the rate of decrease in brittleness is lower compared to other joint orientation angles.

The peak strength and the corresponding failure model of numerical specimens for different joint orientation angles under different intermediate principal stresses are shown in Figs. 17 and 18. At low σ_2/σ_{ci}, especially in uniaxial compression tests, the number of tensile cracks is considerably greater than the shear cracks. As σ_2/σ_{ci} increases, the contribution of shear cracks in the strength and the failure mode increases and the corresponding ratio of shear to tensile crack increases.

The highest uniaxial and biaxial compressive strengths

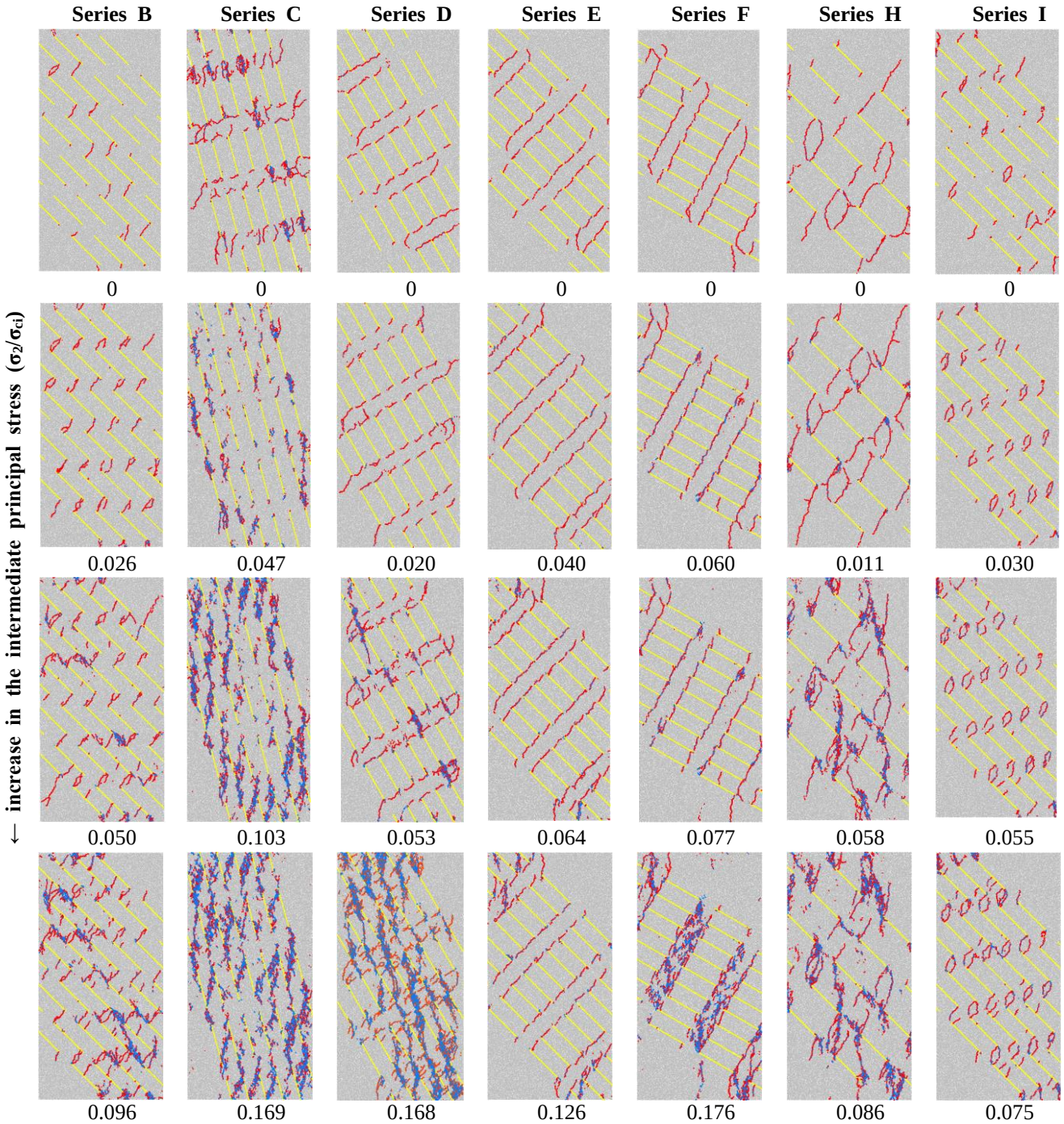

Fig. 15 Change of the failure mode with an increase in the intermediate principal stress

occur at β= 0° where all samples failed by breakage through intact material. At β= 15°, the increase in σ_2/σ_{ci} results in the change of failure modes from planar to mixed planar and intact failure and at high lateral stresses to intact failure. At β= 30°, propagation of wing cracks leads to generation of blocks under uniaxial loading condition while the increase in σ_2/σ_{ci} results in the increment in the contribution of intact rock bridges in the failure mode. Therefore, the failure modes change to mixed block rotation and planar failure and then at high confining stresses to mixed block rotation failure and intact failure. At β= 45°, in all studied σ_2/σ_{ci} values, failure occurs by generation of blocks and the lowest strength is recorded in this joint orientation. At β= 60° and 75°, at low lateral stresses samples fail in block rotation mode and the increase in the lateral stress results in contribution of intact rock material in the strength and the failure mode. At β= 90°, intact material between fractures controls the failure mechanism. However, the strength is considerably lower than that of β= 0° due to initiation of cracks from fracture tips. This difference decreases with an increase in the σ_2/σ_{ci}. It is noteworthy that the increase in σ_2/σ_{ci} results in the decrease of strength anisotropy at different joint orientations.

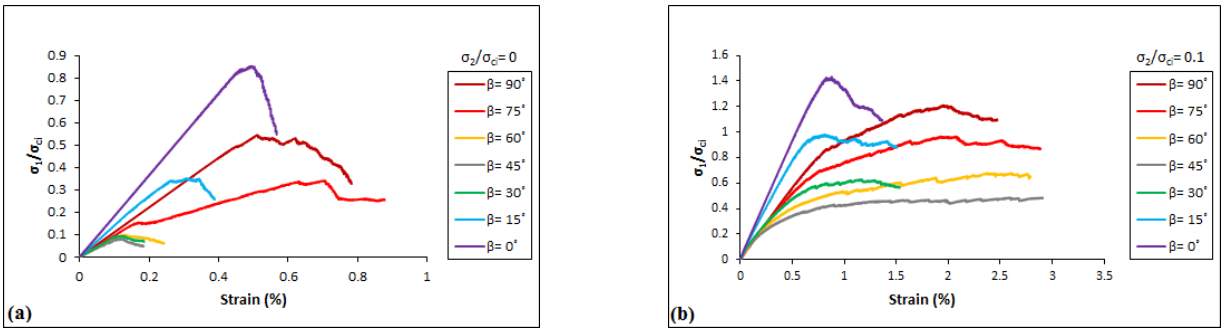

(a) (b)

Fig. 16 Influence of intermediate principal stress on the strain-stress curve and the post-peak behaviour: (a) σ_2/σ_{ci}= 0 and (b) σ_2/σ_{ci}= 0.1

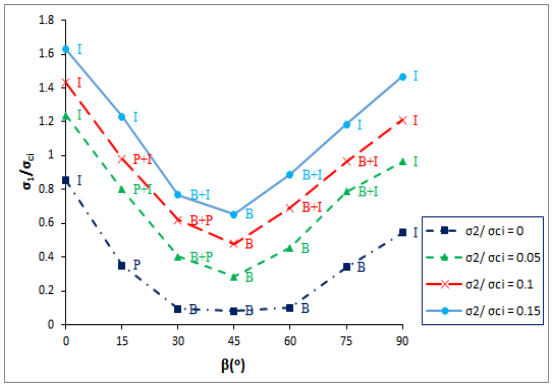

Fig. 17 Effect of joint orientation and intermediate principal stress on the strength of non-persistent samples

It is noteworthy that that at the uniaxial compression tests, there is a slight difference in the strength of specimens in the range of $30^\circ \leq \beta \leq 60^\circ$, where all samples failed in block rotation failure mode, while, the lowest strength is observed at $\beta = 45^\circ$with an increase in the intermediate stress (Fig. 17). This due to generation of planar failure surfaces at $\beta = 30^\circ$ and generation of step failure paths at $\beta = 60^\circ$ with an increase in the intermediate principal stress (Fig. 18).

Investigation of the failure modes of samples at different orientations and σ_2/σ_{ci} (Fig. 18) shows different zones in the failure mode of samples at different joint orientations. At β close to 0º, samples fail in intact failure mode and an increase in σ_2/σ_{ci} results in the increase of intact failure zone. At β around 15º, there is a transition from intact to block rotation failure mode and samples may fail in planar mode depending on the applied σ_2/σ_{ci}. There is a decreasing trend in the strength of material in this zone. At $30 \leq \beta \leq 75$, samples fail in block rotation mode (or step-path failure depending on the joint step angle γ) and the minimum strength occurs in this range. At β greater than 75º, there is a transition zone in the failure mode from block rotation to intact rock bridges failure zone where the size of this zone increases considerably with an increase in σ_2/σ_{ci} due to increase in the contribution of intact rock bridges in the strength.

The other important parameter in studying the mechanical behaviour of jointed rock masses is the deformation modulus. The measured deformation modulus at different joint orientation angles were normalised by that of the intact rock materials and the results are presented in Fig. 19. The deformation modulus decreases with the increase in β from 0° to $45^\circ$and reaches the minimum value at $\beta = 45^\circ$. Increase of β from 45° to 90° results in the increase in the deformation modulus.

The finding of this study clearly show that the failure mode and strength of non-persistent materials are mainly dependent on the joint orientation and the applied confining stress. Identification of the failure zones can provide a useful guideline for estimation of the mechanical behaviour of these materials. However, this requires a large set of experiments with different joint configurations which is recommended for future studies.

5. Conclusions

In this study, the mechanical behaviour of non-persistent jointed rock masses under uniaxial and biaxial loading conditions were numerically studied using the PFC2D. Numerical simulation of the mechanical behaviour of intact rock and jointed rock masses under biaxial and triaxial loading conditions have been problematic in the past due to shortcomings of bonding approaches (contact bond and parallel bond). However, these problems have been solved with the development of the flat-joint model. In this paper, the effect of the joint orientation and confining stress on the

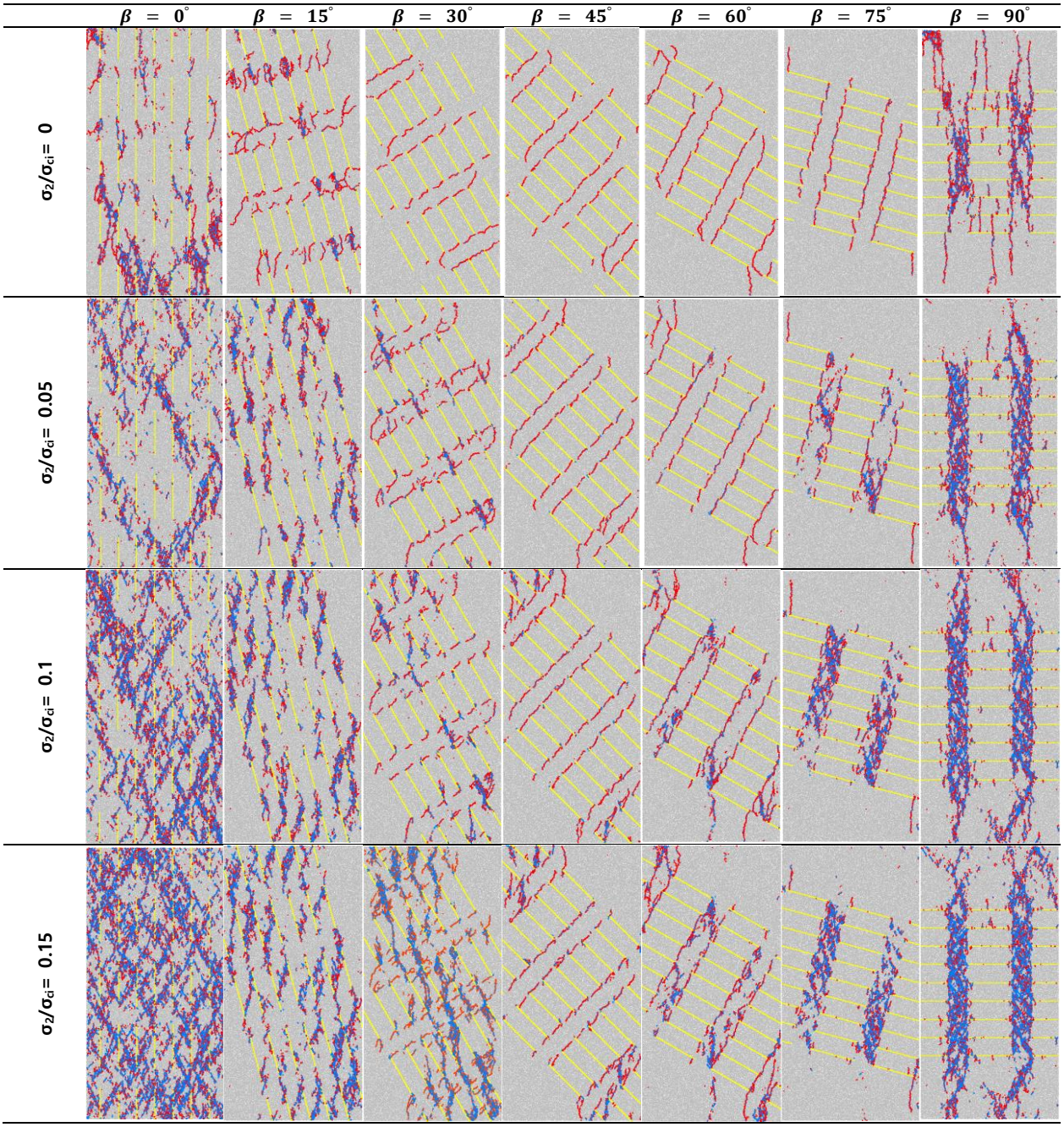

Fig. 18 Effect of joint orientation and intermediate stress on the failure mode of non-persistent samples

strength, deformation modulus, failure mode and the post-peak behaviour were studied using the flat-jointed model. First, a validation study was carried out through a comparative analysis against undertaken physical uniaxial and biaxial compression experiments. The micro-properties of the numerical model (flat-joint for simulation of the intact material and smooth-joint for simulation of the rock joints) were calibrated against physical properties of the intact material and the planar joint. Then, ten series of non-persistent jointed numerical samples with different joint configurations were generated and results were compared with those of experimental tests. The results showed a good agreement with physical experiments in terms of strength and failure modes under different confining stresses. Finally, parametric study on the effect of joint orientation β and confining stress on the mechanical behaviour of non-persistent were carried out. The results show a significant anisotropy in the strength of non-persistent jointed rock mass at different joint orientations. The highest strength and deformation modulus occur at β= 0° while the lowest values were recorded at β= 45°. It was found that the generation and propagation of wing cracks can considerably reduce the strength of material. Four failure zones of intact, transition from intact to block rotation, block rotation and transition to intact failure were identified when the joint orientation was varied from 0° to 90° in these experiments and it was found

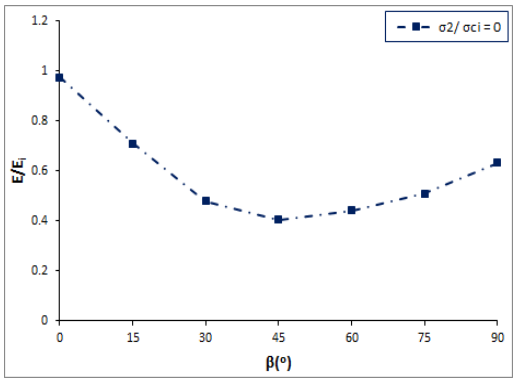

Fig. 19 The effect of joint orientation angle on the deformation modulus

that the applied confining stress can significantly change the size of transition zones. It was found that samples fail in brittle mode at intact failure zone (β close to 0°) while the post-peak behaviour changes to ductile mode at block rotation zone $30 \leq \beta \leq 75$. The increase in the confining stress leads to decrease in brittleness of the rock mass where the post-peak behaviour changes to fully ductile mode at the block rotation zone.

References

Asadizadeh, M., Moosavi M. and Hossaini M.F. (2018), "Investigation of mechanical behaviour of non-persistent jointed blocks under uniaxial compression", *Geomech. Eng.*, **14**(1), 29-42. http://doi.org/10.12989/gae.2018.14.1.029.

Bahaaddini, M. (2014), "Numerical study of the mechanical behaviour of rock joints and non-persistent jointed rock masses", Ph.D. thesis, University of New South Wales, Australia.

Bahaaddini, M. and Rahimi, M. (2018), "Distinct element modelling of the mechanical behaviour of intact rocks using voronoi tessellation model", *Int. J. Min. Geo-Eng.*, **52**(1), 61-68. https://doi.org/10.22059/ijmge.2017.240741.594694.

Bahaaddini, M., Hagan, P.C. Mitra, R. and Hebblewhite, B.K. (2015), "Parametric study of smooth joint parameters on the shear behaviour of rock joints", *Rock Mech. Rock Eng.*, **48**, 923-940. https://doi.org/10.1007/s00603-014-0641-6.

Bahaaddini, M., Sharrock, G. and Hebblewhite, B.K. (2011), "A comparison of physical and numerical experiments on artificial jointed rock masses using PFC3D", *Proceedings of the 2th International FLAC/DEM Symposium*, Melbourne, Australia.

Bahaaddini, M., Sharrock, G. and Hebblewhite, B.K. (2013), "Numerical investigation of the effect of joint geometrical parameters on the mechanical properties of a non-persistent jointed rock mass under uniaxial compression", *Comput. Geotech.*, **49**, 206-225. https://doi.org/10.1016/j.compgeo.2012.10.012.

Bahaaddini, M., Sharrock, G., Hebblewhite, B.K. and Mitra, R. (2012a), "Direct shear tests to model the shear behavior of rock joints by PFC2D", *Proceedings of the 46th US Rock Mechanics/Geomechanics Symposium*, American Rock Mechanics Association.

Bahaaddini, M., Sharrock, G., Hebblewhite, B.K. and Mitra, R. (2012b), "Statistical analysis of the effect of joint geometrical parameters on the mechanical properties of non-persistent jointed rock masses", *Proceedings of the 46th US Rock Mechanics/Geomechanics Symposium*, Chicago, USA, American Rock Mechanics Association.

Bahaaddini, M., Sheikhpourkhani, A.M. and Mansouri, H. (2019), "Flat-joint model to reproduce the mechanical behaviour of intact rocks", *Eur. J. Environ. Civil Eng.*, 1-22. https://doi.org/10.1080/19648189.2019.1579759.

Bobet, A. and Einstein, H.H. (1998), "Fracture coalescence in rock-type materials under uniaxial and biaxial compression", *Int. J. Rock Mech. Min. Sci.*, **35**(7), 863-888. https://doi.org/10.1016/S0148-9062(98)00005-9.

Brown, E.T. (2008), "Estimating the mechanical properties of rock masses", *Paper presented at the Proceedings of the First Southern Hemisphere International Rock Mechanics Symposium*, Perth, 16-19. September.

Cao, R.H. and Lin, H. (2017), "Experimental and numerical study of failure behavior and energy mechanics of rock-like materials containing multiple joints", *Adv. Mater. Sci. Eng.*, **2017**, https://doi.org/10.1155/2017/6460150.

Chen, X., Liao, Z. and Peng, X. (2012), "Deformability characteristics of jointed rock masses under uniaxial compression", *Int. J. Min. Sci. Technol.*, **22**(2), 213-221. https://doi.org/10.1016/j.ijmst.2011.08.012.

Cho, N., Martin, C.D. and Sego, D.C. (2007), "A clumped particle model for rock", *Int. J. Rock Mech. Min. Sci.*, **44**(7), 997-1010. https://doi.org/10.1016/j.ijrmms.2007.02.002.

Cording, E. and Jamil, M. (1997), "Slide geometries on rock slopes and walls", *Proceedings of the 4th South American Congress on Rock Mechanics*, Santiago.

Cundall, P.A. (2000), "Numerical experiments on rough joints in shear using a bonded particle model", *Proceedings of the Aspects of Tectonic Faulting: In Honour of Georg Mandl*, Springer Berlin Heidelberg, Berlin, Heidelberg, https://doi.org/10.1007/978-3-642-59617-9_1.

Elmo, D., Donati, D. and Stead, D. (2018), "Challenges in the characterisation of intact rock bridges in rock slopes", *Eng. Geology*, **245**, 81-96. https://doi.org/10.1016/j.enggeo.2018.06.014.

Fan, X., Kulatilake, P.H.S.W. and Chen, X. (2015), "Mechanical behavior of rock-like jointed blocks with multi-non-persistent joints under uniaxial loading: a particle mechanics approach", *Eng. Geology*, **190**, 17-32. https://doi.org/10.1016/j.enggeo.2015.02.008.

Han, G., Jing, H., Jiang, Y., Liu, R., Su, H. and Wu, J. (2018), "The effect of joint dip angle on the mechanical behavior of infilled jointed rock masses under uniaxial and biaxial compressions", *Processes*, **6**(5), 49. https://doi.org/10.3390/pr6050049.

Itasca Consulting Group. Inc, (2015), "PFC (particle flow code is 2 and 3 dimensions)", version 5 user's manual, Minneapolis, Minnesota.

Jamil, S.M. (1992), "Strength of non-persistent rock joints", PhD Thesis, University of Illinois.

Jennings, J. (1970), "A mathematical theory for the calculation of the stability of slopes in open cast mines", *In: Planning Open Pit Mines, Proceedings, Johannesburg, AA Balkema Cape Town*, **21**, 87-102.

Kachanov, M. (1987), "Elastic solids with many cracks: a simple method of analysis", *Int. J. Solid. Struct.*, **23**(1), 23-43. https://doi.org/10.1016/0020-7683(87)90030-8.

Mas Ivars, D., Pierce, M.E., Darcel, C., Reyes-Montes, J., Potyondy, D.O., Paul Young, R. and Cundall, P.A. (2011), "The synthetic rock mass approach for jointed rock mass modelling", *Int. J. Rock Mech. Min. Sci.*, **48**(2), 219-244. https://doi.org/10.1016/j.ijrmms.2010.11.014.

Mughieda, O.S. (1997), "Failure mechanisms and strength of non-persistent rock joints", PhD Thesis, University of Illinois.

Park, C.H. and Bobet, A. (2009), "Crack coalescence in specimens with open and closed flaws: A comparison", *Int. J. Rock Mech. Min. Sci.*, **46**(5), 819-829. https://doi.org/10.1016/j.ijrmms.2009.02.006.

Park, C.H. and Bobet, A. (2010), "Crack initiation, propagation and coalescence from frictional flaws in uniaxial compression", *Eng. Fract. Mech.*, **77**(14), 2727-2748. https://doi.org/10.1016/j.engfracmech.2010.06.027.

Pierce, M., Cundall, P.A. Potyondy, D.O. and Mas Ivars, D. (2007), "A synthetic rock mass model for jointed rock", *In: Rock mechanics: meeting society's challenges and demands*, 341-349.

Potyondy, D.O. (2011), "Parallel-bond refinements to match macroproperties of hard rock", *Proceedings of the 2nd International FLAC/DEM Symposium: Continuum and distinct element modeling in Geomechanics*.

Potyondy, D.O. (2012), "A flat-jointed bonded-particle material for hard rock", *Proceedings of the 46th US rock mechanics/geomechanics symposium*, American Rock Mechanics Association.

Potyondy, D.O. (2015), "The bonded-particle model as a tool for rock mechanics research and application: current trends and future directions", *Geosyst. Eng.*, **18**(1), 1-28. https://doi.org/10.1080/12269328.2014.998346.

Potyondy, D.O. and Cundall, P.A. (2004), "A bonded-particle model for rock", *Int. J. Rock Mech. Min. Sci.*, **41**(8), 1329-1364. https://doi.org/10.1016/j.ijrmms.2004.09.011.

Prudencio, M. (2009), "Study of the strength and failure mode of rock mass with non-persistent joints", PhD Thesis, Catholic University of Chile.

Prudencio, M. and Van Sint Jan, M. (2007), "Strength and failure modes of rock mass models with non-persistent joints", *Int. J. Rock Mech. Min. Sci.*, **44**(6), 890-902. https://doi.org/10.1016/j.ijrmms.2007.01.005.

Renani, H.R., Martin, C.D. and Cai, M. (2019), "An analytical model for strength of jointed rock masses", *Tunn. Undergr. Sp. Tech.*, **94**, 103159. https://doi.org/10.1016/j.tust.2019.103159.

Shemirani, A.B., Haeri H., Sarfarazi V. and Hedayat A. (2017), "A review paper about experimental investigations on failure behaviour of non-persistent joint", *Geomech. Eng.*, **13**(4), 535-570. http://doi.org/10.12989/gae.2017.13.4.535.

Tian, W.L. and Yang S.Q. (2017), "Experimental and numerical study on the fracture coalescence behavior of rock-like materials containing two non-coplanar filled fissures under uniaxial compression", *Geomech. Eng.*, **12**(3), 541-560. http://doi.org/10.12989/gae.2017.12.3.541.

Vergara, M.R., Jan, M.V.S. and Lorig, L. (2016), "Numerical model for the study of the strength and failure modes of rock containing non-persistent joints", *Rock Mech. Rock Eng.*, **49**, 1211-1226. https://doi.org/10.1007/s00603-015-0824-9.

Wong, R.H. and Chau, K. (1998), "Crack coalescence in a rock-like material containing two cracks", *Int. J. Rock Mech. Min. Sci.*, **35**(2), 147-164. https://doi.org/10.1016/S0148-9062(97)00303-3.

Wu, S. and Xu, X. (2016), "A study of three intrinsic problems of the classic discrete element method using flat-joint model", *Rock Mech. Rock Eng.*, **49**, 1813-1830. https://doi.org/10.1007/s00603-015-0890-z.

Yang, S.Q. and Jing, H.W. (2011), "Strength failure and crack coalescence behavior of brittle sandstone samples containing a single fissure under uniaxial compression", *Int. J. Fracture*, **168**, 227-250. https://doi.org/10.1007/s10704-010-9576-4.

Yang, S.Q., Huang, Y.H. and Ranjith, P. (2018), "Failure mechanical and acoustic behavior of brine saturated-sandstone containing two pre-existing flaws under different confining pressures", *Eng. Fract. Mech.*, **193**, 108-121. https://doi.org/10.1016/j.engfracmech.2018.02.021.

Yang, X.X., Jing, H.W. Tang, C.A. and Yang, S.Q. (2017), "Effect of parallel joint interaction on mechanical behavior of jointed rock mass models", *Int. J. Rock Mech. Min. Sci.*, **92**, 40-53. https://doi.org/10.1016/j.ijrmms.2016.12.010.

Yin, P., Wong, R. and Chau, K. (2014), "Coalescence of two parallel pre-existing surface cracks in granite", *Int. J. Rock Mech. Min. Sci.*, **68**, 66-84. https://doi.org/10.1016/j.ijrmms.2014.02.011.

Zhang, Y., Jiang, Y., Shi, X., Yin, Q. and Chen, M. (2020), "Shear failure and mechanical behavior of flawed specimens containing opening and joints", *Geomech. Eng.*, **23**(6), 587-600. http://doi.org/10.12989/gae.2020.23.6.587.

Zhao, W., Huang, R. and Yan, M. (2015), "Mechanical and fracture behavior of rock mass with parallel concentrated joints with different dip angle and number based on PFC simulation", *Geomech. Eng.*, **8**(6), 757-767. http://dx.doi.org/10.12989/gae.2015.8.6.757.

Zhou, C., Xu, C., Karakus, M. and Shen, J. (2018), "A systematic approach to the calibration of micro-parameters for the flat-jointed bonded particle model", *Geomech. Eng*., **16**(5), 471-482. http://doi.org/10.12989/gae.2018.16.5.471.

CC